JPhys Materials

Rare-earth magnetic nitride perovskites

JPhys Materials

OPEN ACCESS

RECEIVED
22 August 2018

REVISED
15 February 2019

ACCEPTED FOR PUBLICATION
19 February 2019

PUBLISHED
21 March 2019

PAPER

Rare-earth magnetic nitride perovskites

José A Flores-Livas[1,5], **R Sarmiento-Pérez**[2], **Silvana Botti**[3], **Stefan Goedecker**[1] and **Miguel A L Marques**[4]

[1] Department of Physics, Universität Basel, Klingelbergstr. 82, 4056 Basel, Switzerland
[2] Department of Chemistry, University of Basel, Klingelbergstr. 80 4056 Basel, Switzerland
[3] Institut für Festkörpertheorie und -optik, Friedrich-Schiller-Universität Jena, Max-Wien-Platz 1, D-07743 Jena, Germany
[4] Institut für Physik, Martin-Luther-Universität Halle-Wittenberg, D-06099 Halle, Germany
[5] Author to whom any correspondence should be addressed.

E-mail: jflores.livas@gmail.com

Keywords: hard-magnetic materials, nitrides, perovskites, rare-earth materials

Supplementary material for this article is available online

Abstract

We propose perovskite nitrides with magnetic rare-earth metals as novel materials with a range of technological applications. These materials appear to be thermodynamically stable and, in spite of possessing different crystal structures and different atomic environments, they retain the magnetic moment of the corresponding elemental rare-earth metal. We find both magnetic metals and semiconductors, with a wide range of magnetic moments and some systems posses record high magnetic anisotropy energies. Further tuning of the electronic and magnetic properties can also be expected by doping with other rare-earths or by creating solid solutions. The synthesis of these exotic materials with unusual compositions would not only extend the accepted stability domain of perovskites, but also open the way for a series of applications enabled by their rich physics.

Introduction

The applications of perovskite materials are unparalleled among the different families of compounds. In fact, many materials with exceptional properties (some of them of enormous technological relevance) exhibit a perovskite-like structure [1–12]. As a few examples, perovskite oxides have been found to be conductive and even high-temperature superconducting [9, 10], they can be used as thermoelectrics [3], for lasing [2, 13] and magnetism [14]. This wide range of applicability arises from the large number of elements that are possible to accommodate in a rather *simple* crystal structure. Furthermore, this structure can easily tolerate distortions from intercalations, dopants and defects [15].

Perovskites have the generic chemical formula ABX_3, where A and B are cationic sites, with B located in the center of a characteristic octahedra of X anions and A occupying the center of the space left between eight of them. While the A and B sites can be occupied by species from a large portion of the periodic table, X is commonly occupied by oxygen or, less frequently, by other chalcogens and some halogens [16]. Other more complex phases also exist such as the oxynitride perovskites, in which oxygen and nitrogen occupy the same sublattice. In fact, these materials are being extensively studied due their interesting optical, photocatalytic, dielectric, and magnetoresistive properties [17]. The O/N ratio in these structures, which allows to tune their electronic properties, can be as low as 0.25% as in $LaWO_{0.6}N_{2.4}$ [17–19]. However, the synthesis of pure nitride perovskites resulted to be a very challenging task, and only one compound ($TaThN_3$ [20]) has been reported up to now.

Indeed, crystals with the ABN_3 stoichiometry are extremely rare regardless of the crystal structure. A simple rule of thumb to understand the singularity of this stoichiometry is to think in terms of the standard oxidation states. In order to achieve overall charge neutrality, a -3 oxidation state of nitrogen requires that the cations must be able to assume very high oxidation states to reach a total cationic valence of $+9$. Such high oxidation states are rarer than those required for oxide perovskites. It is therefore not surprising that the cations in $TaThN_3$ correspond to the region of the periodic table where the highest oxidation states can be found.

Recently, three novel nitride perovskites (along with other ABN_3 non-perovskite low-symmetry crystals) were obtained theoretically [21] with a combination of high-throughput techniques and global structure

Table 1. Calculated saturation magnetization (M_s) for $LnReN_3$ using the LSDA + U approximation and magnetic spin and orbital moment per Ln site. The structure type (P = perovskite, M = monoclinic, O = orthorhombic), space group (Spg) and electronic character (**m**: metal, **s**: semiconductor) information is also included.

Material	Type	Spg		$2\langle s\rangle$ (μ_B)	$\langle l\rangle$ (μ_B)	M_s (MA m^{-1})
$LaReN_3$	P	*Pnma*	**m**	0.0008	0.000 07	0.0001
$CeReN_3$	P	*Pnma*	**m**	0.0642	0.043 20	0.0016
$PrReN_3$	P	*Pnma*	**m**	0.8204	3.332 64	0.6221
$NdReN_3$	P	*Pnma*	**m**	2.1762	4.156 73	0.9574
$PmReN_3$	P	*Pnma*	**m**	3.7600	4.241 44	1.2210
$SmReN_3$	P	*Pnma*	**m**	4.6322	3.724 93	1.2832
$EuReN_3$	O	*Cmcm*	**s**	6.7896	0.012 61	0.7338
$GdReN_3$	P	*Pnma*	**m**	6.6995	0.182 87	1.0708
$TbReN_3$	P	*Pnma*	**m**	5.8292	1.743 32	1.1903
$DyReN_3$	P	*Pnma*	**m**	4.5819	3.628 36	1.2985
$HoReN_3$	P	*Pnma*	**m**	3.1787	4.710 87	1.2558
$ErReN_3$	P	*Pnma*	**m**	2.5378	4.439 85	1.1178
$TmReN_3$	P	*Pnma*	**m**	0.6853	1.394 49	0.3355
$YbReN_3$	M	$C2/c$	**m**	0.2270	0.802 24	0.1225
$LuReN_3$	P	*Pnma*	**m**	0.0008	0.000 03	0.0001

prediction [22, 23]. The three perovskites are $LaReN_3$, $YReN_3$ and $LaWN_3$. As could be expected, all these cations are capable of high oxidation states.

The presence of La in the cationic site A in two of these systems opens up the tantalizing possibility of finding other thermodynamically stable compounds by simply replacing it for other lanthanide cations: it is well known that the strong localization of the 4*f* orbitals of the lanthanides leads to a reduced orbital interaction with other atoms. This implies that there is essentially no effect other than steric in replacing one lanthanide by another, resulting in chemically similar materials but with different electronic and magnetic properties. It is therefore reasonable to expect that $LnReN_3$ and $LnWN_3$ compositions, with Ln = Ce, La, Pr, Nd, Pm, Sm, Eu, Gd, Tb, Dy, Ho, Er, Tm, Yb and Lu, can likewise be stable compounds with perovskite structures.

It has been reported experimentally that oxide perovskites with lanthanide cations show interesting magnetic and electronic properties [24–26]. For instance $LaNiO_3$ and $LaFeO_3$, which are isostructural to $CaTiO_3$, are stable structures with exceptional magnetic and electronic properties [27]. These lanthanide perovskites exhibit temperature-depending physical properties like metal-insulator or paramagnetic-ferromagnetic transitions [24, 27]. Other lanthanide-transition metal oxide perovskites such as $LnCrO_3$, $LnVO_3$, $LnRhO_3$ and $LnAlO_3$ have been scarcely studied. However, similar materials such as perovskite $LaCoO_3$ show Bose–Einstein condensation of excitons into the lowest energy state (also called the excitonic magnet) [28]. This effect stems from the unique structure-electron-host configuration, making this type of materials a new playground to explore further technological applications.

In this work we study via first-principles calculations whether nitrides including rare-earth metals are chemically stable and if they form perovskite structures. We report that intriguing magnetic properties can arise in these novel and unique materials.

Results

Crystal structure and stability

We consider Re and W cations in the B-site, while for the A-site the entire lanthanide series is explored. Our study includes three perovskite prototypes (with space group $R\bar{3}c$, $R3c$ and *Pnma*), which allow for the usual octahedra tilting and distortions. Two other prototypes included in our study, and that do not exhibit the characteristic anion octahedra, are an orthorhombic and a monoclinic crystal structure with space group *Ama*2 and $C2/c$. These structures were chosen as they turned out to be the the lowest in energy in our previous study of nitride perovskites [21]. We then fully relaxed all structures allowing for spin-polarization, and calculated the energies of formation and other properties.

The distances to the ternary convex hulls of stability for the resulting structures show that all stoichiometries considered in this work are thermodynamically stable. All the values are tabulated in the supplemental information (SI) available online at stacks.iop.org/JPMATER/2/025003/mmedia. Moreover, the (negative) distances to the convex hull are rather large (mostly between 100 and 300 meV atom^{-1}), and therefore, larger than the typical errors of the theoretical framework used for the calculations on this work. This make us

Table 2. Calculated saturation magnetization (M_s) for $LnWN_3$ using the LSDA + U approximation and magnetic spin and orbital moment per Ln site. The structure type (P = perovskite, M = monoclinic, O = orthorhombic), space group (Spg) and electronic character (**m**: metal, **s**: semiconductor) information is also included.

Material	Type	Spg		$2\langle s\rangle$ (μ_B)	$\langle l\rangle$ (μ_B)	M_s (MA m^{-1})
$LaWN_3$	P	*R3c*	**s**	0.0000	0.000 00	0.0000
$CeWN_3$	P	*Pnma*	**m**	0.0756	0.061 55	0.0021
$PrWN_3$	M	*C2/c*	**s**	0.7862	3.302 20	0.4533
$NdWN_3$	M	*C2/c*	**s**	2.2069	4.115 46	0.7099
$PmWN_3$	M	*C2/c*	**s**	3.7260	4.332 33	0.9154
$SmWN_3$	M	*C2/c*	**s**	4.8440	3.358 19	0.9029
$EuWN_3$	P	*R3c*	**s**	4.9425	2.351 47	0.7990
$GdWN_3$	M	*C2/c*	**s**	6.7944	0.063 84	0.7978
$TbWN_3$	M	*C2/c*	**s**	5.8173	1.696 20	0.8827
$DyWN_3$	M	*C2/c*	**s**	4.7049	3.275 75	0.9437
$HoWN_3$	M	*C2/c*	**s**	3.2564	4.778 50	0.9554
$ErWN_3$	M	*C2/c*	**s**	2.5439	4.967 83	0.8979
$TmWN_3$	M	*C2/c*	**s**	1.3418	3.100 13	0.5352
$YbWN_3$	P	*R3c*	**s**	0.0019	0.015 11	0.0025
$LuWN_3$	M	*C2/c*	**s**	0.0001	0.000 05	0.0000

Table 3. Calculated saturation magnetization (M_s) and first-moment uniaxial magnetic anisotropy for outstanding nitride perovskites and selected known hard magnets, experimental values are taken from page 377 of [39].

	Calculated		Experimental		
Material	M_s (M A m^{-1})	K_1 (K Jm^{-3})	M_s (MA m^{-1})	K_1 (K Jm^{-3})	Easy axis
$SmCo_5$	1.2	21 800	0.86	17 200	[001]
YCo_5	0.95	7071	0.85	6500	[001]
Co	1.55	250	1.44	410	[001]
$NdReN_3$	0.95	54 300	—	—	[001]
$DyReN_3$	1.29	36 525	—	—	[100]
$PmWN_3$	0.91	39 173	—	—	[001]
$HoWN_3$	0.95	28 580	—	—	[100]

Table 4. Calculated saturation magnetization (M_s), first-moment uniaxial magnetic anisotropy and easy axis of magnetization for selected structures. Energy difference in mHa atom^{-1} between ferromagnetic and antiferromagnetic (AF1) configurations (negative values means ferromagnetic configuration is the lowest), see figure 7 for AF details.

	MAE			
Material	M_s (M A m^{-1})	K_1 (K Jm^{-3})	Easy axis	Energy difference (mHa atom^{-1})
$NdReN_3$	0.95	54 300	[001]	−3.584
$DyReN_3$	1.29	36 525	[100]	−0.015
$PmWN_3$	0.91	39 173	[001]	−0.707
$HoWN_3$	0.95	28 580	[100]	−1.271

confident that these compositions can indeed be synthesized experimentally under certain thermodynamic conditions.

Tables 1 and 2 summarize the crystal types and symmetries of the lowest-energy configuration found for each composition. Interestingly, many of the compounds adopt a perovskite structure as their most stable configuration, which is particularly evident when Re occupies the B-site, with the *Pnma* structure dominating for 13 rare-earth elements. For W, on the other hand, only La, Ce and Yb crystallize in a perovskite structure, with the remaining 12 cases adopting a monoclinic (*C2/c*) phase. The most relevant structures are depicted in figure 1, and the crystallographic details are available in the supplemental information.

The volume per formula unit for each system is shown in figure 2. The experimental volume per atom of the corresponding lanthanide elemental metal [29] is shown as well for comparison. Clearly, the volume for each

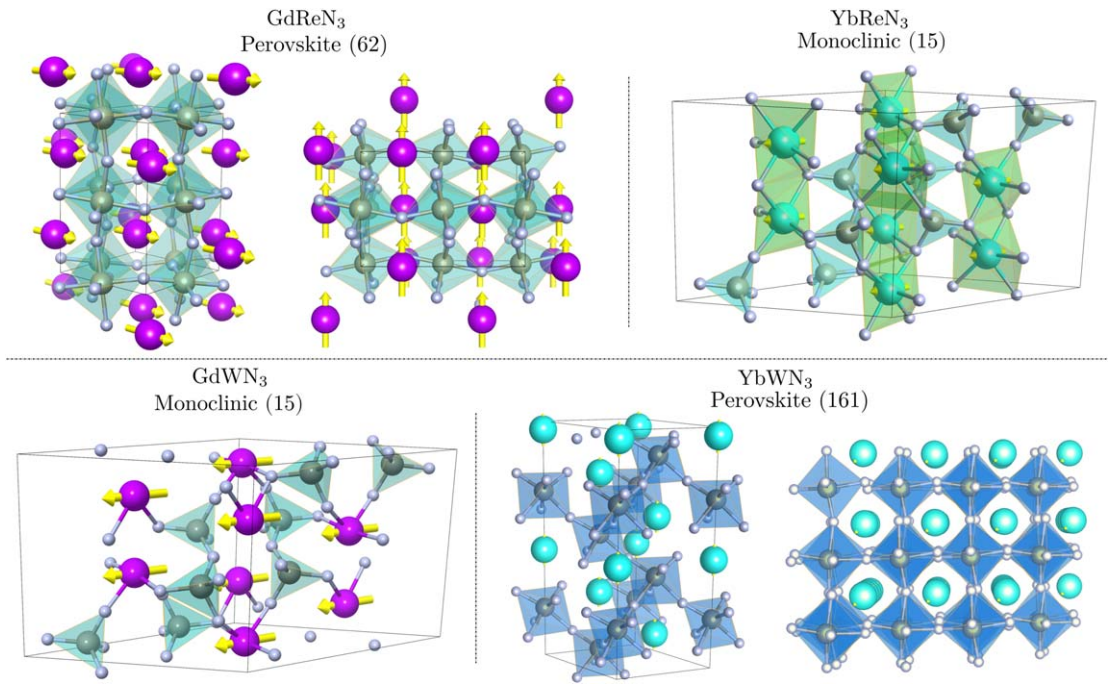

Figure 1. Lowest energy crystal structures. The common perovskite structure (*Pnma*, space group #62, top left) occurs for the vast majority of lanthanides with Re in the B sites, while the second (*R*3*c*, space group #161, bottom right) is the ground state for $LaWN_3$, $EuWN_3$, and $YbWN_3$. The first monoclinic phase (*C*2/*c*, space group #15, bottom left) is reported for the vast majority of systems with W in the B sites, while the second (*C*2/*c*, space group #15, top right) appears for $YbReN_3$. The coordination number of the atoms in the B-site is different for these two structures. Arrows are located at the lanthanide sites and point in the direction of the magnetization, while their length reflects the site-magnetization.

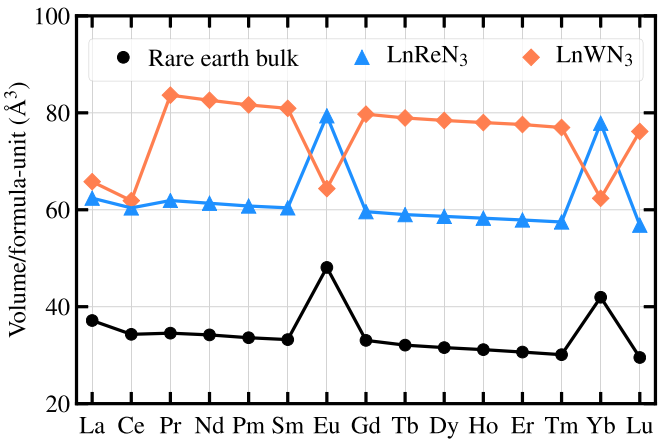

Figure 2. Calculated equilibrium volume per formula unit as a function of the lanthanide cation for $LnReN_3$ (triangles) and $LnWN_3$ (diamonds). For comparison the bulk volume per atom of the corresponding lanthanide elemental metal is depicted in black circles.

nitride compound follows the trend of the elemental substances: volume decreases with atomic number for both $LnReN_3$ and $LnWN_3$. Striking to the eye are the outlier cases of Eu and Yb. This is due to the fact that these two elements are known to assume divalent states [30], in contrast to the other lanthanides that usually form trivalent ions. We would like to point out that the volume is fundamental in understanding the electronic and magnetic properties of these materials (see next section).

Electronic structure

Figures 3 and 4 show the computed spin-polarized density of states for all $LnReN_3$ and $LnWN_3$ compounds. Interestingly, $EuReN_3$ is a semiconductor while the remaining 14 $LnReN_3$ systems are metallic. W, in contrast, shows the tendency to form insulating structures, with the sole exception of $CeWN_3$. There is clearly a

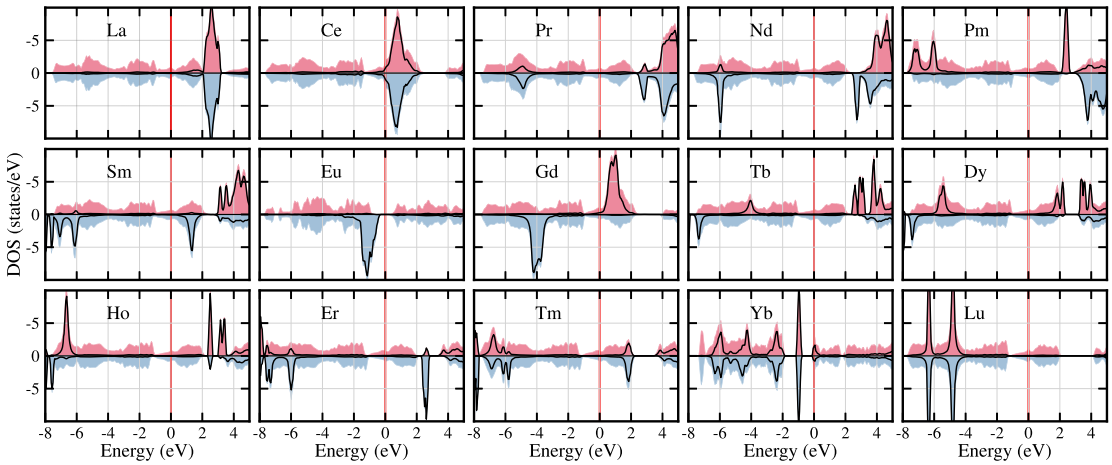

Figure 3. LSDA + U spin-polarized density of states (including spin–orbit coupling) for the $LnReN_3$ compounds. In each panel the thick-black line depicts lanthanide states. The Fermi level is located at 0 eV. With the exception of Eu, all compounds form metallic phases.

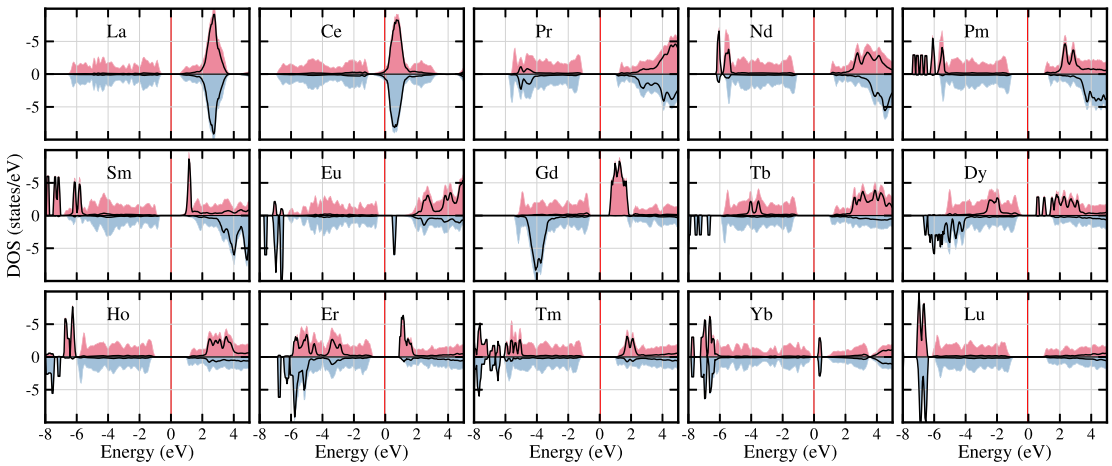

Figure 4. LSDA + U total spin-polarized density of states (including spin–orbit coupling) for $LnWN_3$ compounds. In each panel the thick-black line depicts lanthanide states. The Fermi level is located at 0 eV. Semiconducting phases are found for the entire series with the exception of Ce.

correlation between volume and the electronic character: small volumes lead to a metallic character while more open frameworks tend to yield semiconducting systems.

Most systems exhibit a large magnetic moment, as can be seen from the difference between the up and down densities of states. The exceptions happen at the beginning and the end of the Ln series, where this difference vanishes. In these figures the black lines correspond to the Ln partial density of states, allowing us to observe how the hybridization between 5*d*-states (Re/W), *p*-states (N) and 4*f*–Ln takes place. As expected, all large peaks in the density of states correspond to the localized 4*f*–Ln states. Moreover, another important consequence of having rare-earth atoms occupying the perovskite A-sites, is that they interact, electronically, very little with the surrounding environment. Clearly, the correlated (atomic-like) 4*f* electrons remain localized in the vicinity of the valence band, so we can expect that their magnetic properties closely resemble those in the free atoms.

Magnetic properties

It is well known that standard Kohn–Sham DFT with semi-local approximations to the elusive exchange-correlation functional includes a self-interaction error and, since this error increases with the electron localization, its contribution has substantial effects for 4*f*-electrons. This situation is particularly severe for systems with partially occupied *d* or *f* shells and may lead, e.g. to incorrect metallic ground states for insulating

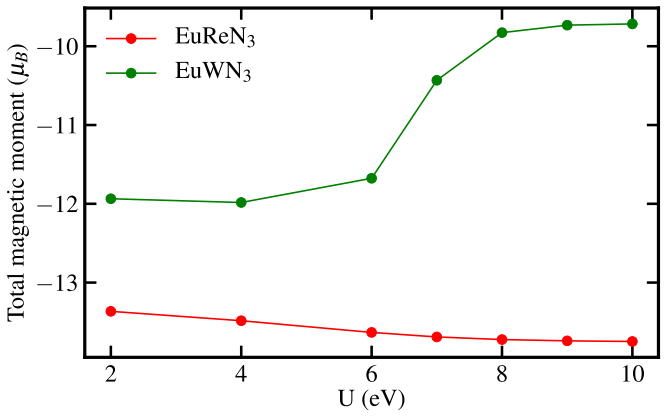

Figure 5. Variation of the total magnetization for two test compounds ($EuReN_3$ and $EuWN_3$) as a function of the parameter U. The magnetic moment remains constant for $U > 8$ eV.

systems. Hybrid functionals, which incorporate a fraction of exact-exchange to the Kohn–Sham energy, partially correct this self-interaction error. Another existing approach to alleviate this problem, is to apply locally a Hubbard U to certain atomic sites. We decided therefore to use the LSDA + U formalism in our calculations of magnetic properties. For the Hubbard term we used the most general version that includes independent U and J parameters [31]. We also used the fully localized limit for double-counting [32, 33], and the Perdew–Wang parametrization [34] for the LSDA.

Unfortunately, a remaining concern is the dependence of the results on the on-site Coulomb repulsion U and the exchange parameter J. Extensive studies have shown that in principle the dependence on such *adjustable* parameters can be attenuated by considering how ground state properties like the electronic gap, magnetic moment and charge distribution, are affected by U [35], and compared to well established experimental values (see for instance [36]). Since we are dealing here with the prediction of novel materials, we can not compare to experiments. We decided therefore to consider the dependence of the electronic band gap and the magnetic moments on U for two systems as measure to determine a suitable value for U. Figure 5 shows the dependence of the total magnetic moment on the value of U for two representative perovskites belonging to the $LnReN_3$ and the $LnWN_3$ families. From the results we can observe that a value of $U = 8$ eV can provide a realistic description of these systems, as the magnetic moment does not changes anymore upon increase of U. Note that this value has also been reported for similar systems ($LaNiO_3$) [37].

Figure 6 summarizes the calculated saturation magnetization (M_s), defined as the total magnetic moment per volume, as a function of the lanthanide species. Numerical data is also summarized in tables 1 and 2. The total magnetic moment for both families of compounds increases according to the number of unpaired-electrons in the 4*f*-shell of the Ln atom. The maximum can therefore be found for $GdReN_3$ and $GdWN_3$, as Gd has the largest number of unpaired electrons. It is important to mention that the entire magnetization is provided solely by the Ln cation, as there are no induced moments on the 5*d* atoms (Re and W).

The lanthanide series can be considered as divided in two blocks according to their magnetic properties: first, La, Ce, Pr, Nd, Sm and Eu, which are known as the light rare-earth elements, are expected to show weak ferromagnetism. The heavy rare-earths, i.e. elements from Gd to Yb, on the other hand, having more than half of their 4*f*-electron shell occupied, are ferromagnetic at low temperatures in their elementary phases. This also seems to be the case in nitrides, as seen in figure 6 and in tables 1 and 2.

To evaluate the potential applicability of these systems as hard magnets we need to estimate the required energy to rotate the magnetization from its ground-state direction, called the easy axis, to the direction of maximum energy, the hard axis. This quantity is called the magnetocrystalline anisotropy energy (MAE). Here we estimated the first moment of the uniaxial magnetic anisotropy defined as

$$K_1 = |E^{\text{tot}}_{[100]} - E^{\text{tot}}_{[001]}|, \tag{1}$$

where $E^{\text{tot}}_{[100]}$ and $E^{\text{tot}}_{[001]}$ are the total energies calculated with the spin-orientation along the [100] and [001] directions. The obtained values for selected perovskite systems are condensed in table 3. For Re-nitrides, Nd and Dy create a large anisotropy while maintaining good levels of saturation magnetization. For W-nitrides, Pm, Sm and Ho are examples of compounds that if synthesized could become hard-magnets. The same table includes values of benchmarked compounds in order to test our MAE estimation (see the appendix). As we can see, these materials have values of the magnetization and MAE of magnitude comparable to the best known hard-magnets [38]. The comparison with the state-of-the-art hard-magnet, $Nd_2Fe_{14}B$ is striking. The compound has

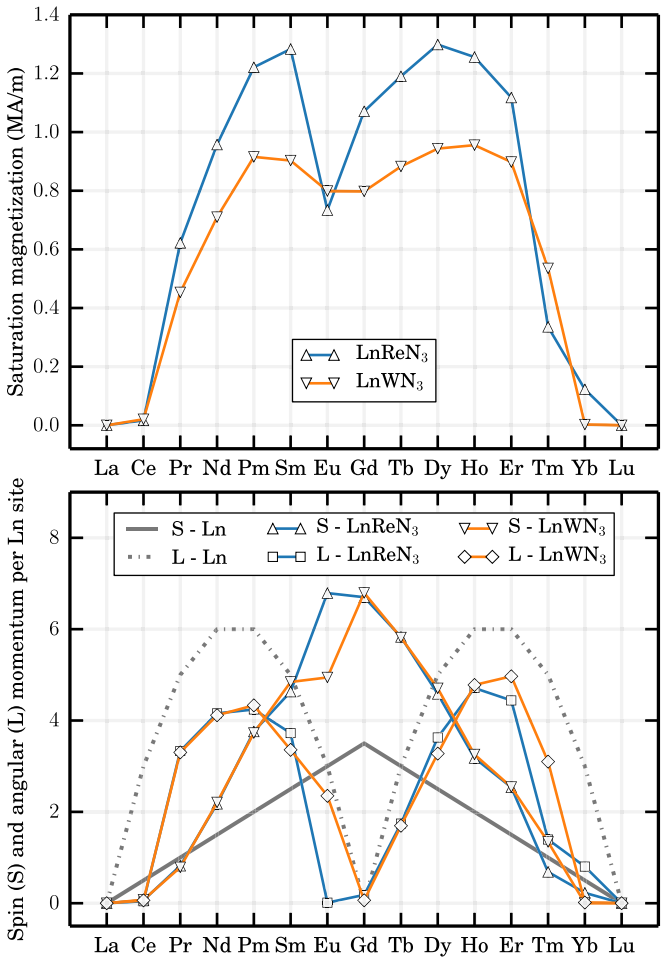

Figure 6. Calculated saturation magnetization (M_s) (upper panel) and magnetic spin (S) and orbital (L) momentum per Ln site for $LnReN_3$ (diamonds) and $LnWN_3$ (triangles) using LDA + U.

$M_s = 1.28$ MA m^{-1} at 300 K and $K_1 \sim 4900$ K J m^{-3} [39], the values of the systems presented in this work are, if not superior, at least comparable to the Nd-based magnets.

As we are dealing with the prediction of magnetic materials, it is pertinent to check the magnetic order of the phases. In order to compare the total energies of ferromagnetic and antiferromagnetic configurations, we created supercells [40] with antiferromagnetic AF1 spin configurations for $NdReN_3$, $DyReN_3$, $PmWN_3$ and $HoWN_3$ (see the supercell configurations in figure 7). The results of calculations of saturation magnetization, magnetic anisotropy, and easy axis of magnetization for the antiferromagnetic configurations are summarized in table 4. In all these cases we found that the ferromagnetic configuration was energetically lower (see table 4). These calculations were performed using the full-potential linearized augmented plane-wave (FP-LAPW) setup as implemented in the ELK code. We used a fully relativistic scheme (i.e. including spin–orbit coupling and non-collinear spin), together with a on-site Coulomb repulsion U and an exchange parameter J, as defined above.

Discussion

Several important conclusions can be drawn from our results. First let us discuss the possibility of the synthesis of these systems. As indicated before, many of the compounds (and in particular with the light rare-earth elements) are well below the respective convex hull of stability. Taking into account the typical errors of energy of formation that can be expected in DFT calculations [41, 42], we can affirm that a large majority of these compositions (if not all) can indeed be produced under attainable thermodynamic conditions.

Moreover, we performed phonon calculations in the frozen phonon approximation, using PHONOPY [43] and forces from VASP. This calculation resulted quite challenging. We restricted the convergence of the supercell to a maximum of 600 atoms per cell (approximately 1000 electron system). Furthermore, to alleviate the computational burden, we had to resort to *spin-unpolarized* calculations. For this reasons we decided to focus

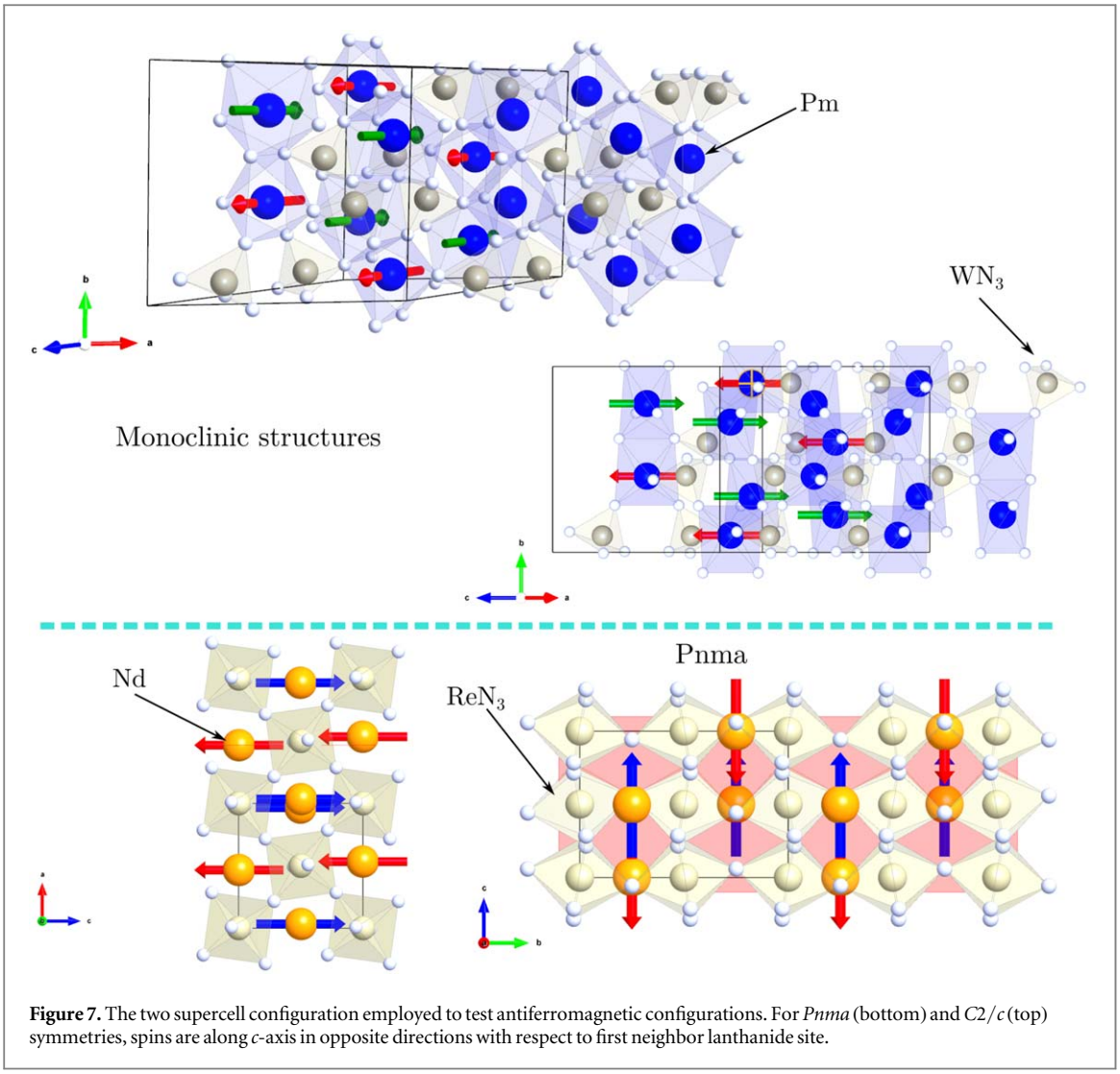

Figure 7. The two supercell configuration employed to test antiferromagnetic configurations. For *Pnma* (bottom) and *C*2/*c* (top) symmetries, spins are along *c*-axis in opposite directions with respect to first neighbor lanthanide site.

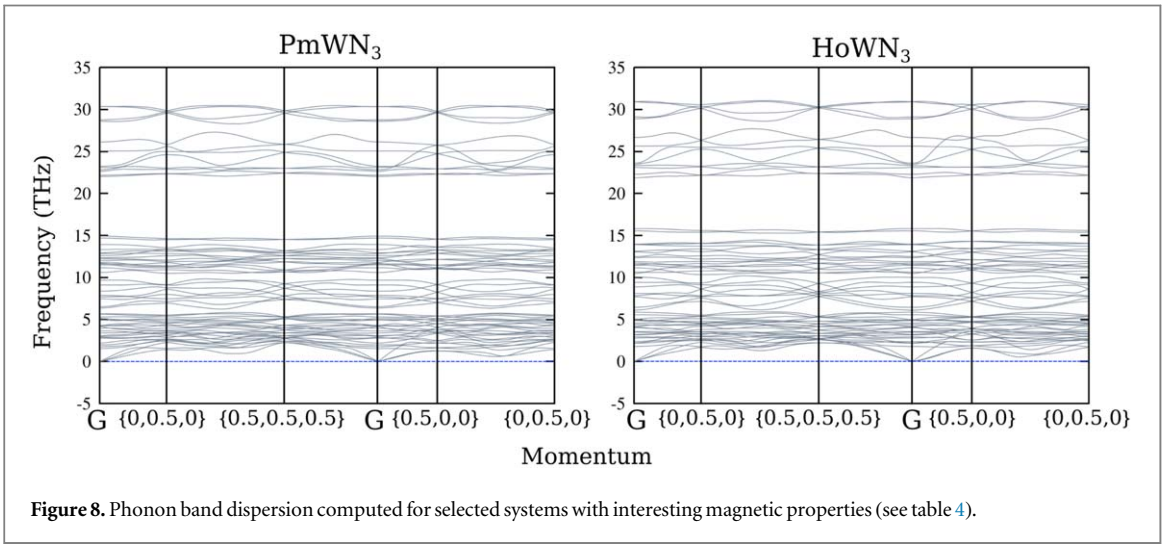

Figure 8. Phonon band dispersion computed for selected systems with interesting magnetic properties (see table 4).

only on two interesting materials. Figure 8 display the phonon band dispersion for selected material predictions. The two compounds containing W (*C*2/*c* space group symmetry) are dynamically stable and both have phonon frequencies in a similar range.

From the electronic and magnetic point of view, several of our systems are extremely interesting and could find their way into several technological applications. Let us give a few examples.

Eu is at the limit of weak magnetism, where spin-fluctuations increase and make all Eu-compounds very interesting for many electronic applications. Our nitrides (both Re- and W-based) with Eu have considerable values of saturation magnetization, in contrast to Eu-oxides, which have the tendency to form antiferromagnetic configurations. For instance, the calculated saturation magnetization for $EuReN_3$ is 0.75 MA m^{-1}. Since $EuReN_3$ has a non-cubic crystal symmetry and Eu has large values of angular momentum, there is a considerable spin–orbit coupling and rather large magnetic anisotropy energy. This is especially true when compared to the widely used oxide-ferrite-based magnets, such as $BaFe_{12}O_{19}$ with $M_s = 0.38$ MA m^{-1} and $K_1 \sim 330$ KJ m^{-3}. The compound $EuReN_3$ could therefore have potential uses as a semiconducting hard magnet, or as a spin filter [44].

The material $TbReN_3$, on the other hand, exhibits outstanding values of anisotropy and magnetization comparable to early 3*d*-row elements. Other systems such as $NdReN_3$and $DyReN_3$show as well extremely high values for these quantities. It is not only interesting to further study these systems to understand how such values are attained (especially of the record magnetic anisotropy energy), but also as they may have practical applications as metallic permanent magnets. As for possible applications, it is important to mention one possible obstacle: although we did not carried out calculations to estimate the Curie temperature (T_c), we expect it to be rather low (well below room temperature) for the compounds predicted in this work. However, there are suitable ways to increase the T_c for these compounds such as incorporating other magnetic elements or doping with magnetic impurities.

Nitrides containing mid-series lanthanides such as Gd, Tb and Dy together with Re, show values of saturation magnetization comparable to strong ferromagnets. As for these elements the orbital moment vanishes, the magnetic anisotropy energy is extremely low, becoming easy to demagnetize. A possible *niche* of applications for this class of materials lies in exploiting its strong ferroelectricity and piezoelectric effects [45].

In summary, we predicted novel perovskite nitrides with magnetic lanthanide cations in their sub-lattices. These compounds are thermodynamically stable and, due to the intrinsic diversity of the lanthanide 4*f*-electrons, they exhibit a variety of electronic and magnetic properties. It is clear that their successful synthesis would enlarge the palette of applications of perovskites. Finally, we certainly expect that properties of these materials could be modified by doping or by creating solid solutions between the different rare-earth nitrides. This opens numerous possibilities to further tune and enhance their electronic and magnetic properties and with that push further the limits of nitride materials.

Methods

All structural relaxations were evaluated within density functional theory (DFT) with the Perdew–Burke–Erzernhof (PBE) [46] approximation to the exchange-correlation functional. A plane wave basis-set with cutoff energy of 820 eV was used to expand the wave-functions together with the projector augmented wave (PAW) method as implemented in the Vienna *ab initio* Simulation Package VASP [47]. Formation energies and distances to the convex hulls of stability (at 0 K) were calculated with the pymatgen python package [48]. For compatibility with the Materials Project database, we used the PAW data sets of version 5.2 supplied with VASP. Geometry relaxations were performed allowing for spin-polarization and starting from a ferromagnetic alignment with tight tolerance criteria for the convergence (forces on the atoms less than 5 meV $Å^{-1}$). Once the structures were relaxed, all magnetic calculations were performed using the full-potential linearized augmented plane-wave (FP-LAPW) method as implemented within the ELK code [49, 50]. We took into account spin–orbit coupling and performed fully non-collinear magnetic calculation. Finally, the potential and density were expanded in plane-waves with a cutoff of $|\mathbf{G}| = 20/a_0$, and we set $R_{\text{min}} \times |\mathbf{G} + \mathbf{k}|$ to 8, where R_{min} is the smallest muffin-tin radius. The maximum angular momentum l for the expansion of the wave-function inside the muffin-tins was set to 10. The muffin-tin radii and k-point grids are automatically determined by the code. All the above mentioned parameters are set automatically by invoking 'highq = true' in the ELK input file.

Acknowledgments

JAF-L acknowledges computational resources under the project (s752) from the Swiss National Supercomputing Center (CSCS) in Lugano and resources in sciCORE, scientific computing center at University of Basel. MALM acknowledges partial support from the DFG through project SFB-762. This research was supported by the NCCR MARVEL, funded by the Swiss National Science Foundation.

Appendix. Benchmark of magnetic anisotropy energy calculations

Magnetic anisotropy benchmark calculations were conducted for $SmCo_5$, YCo_5 (two important magnets showing high coercitivity) and hcp-Co in order to estimate the numerical accuracy of our approximations. The first two systems require the use of a Coulomb on-site U for Sm and Co. For $SmCo_5$ the fully-localized limit double counting correction method and a on-site value of 8 eV and a J of 0.5 eV was used. For YCo_5, the around mean filed correction for the double counting was used, together with a U of 2 eV and J of 0.8 eV for Co. Figure A1 shows the number of k-points necessary to converge the MAE for the above mentioned compounds using their experimental volume. As alluded above, MAE is defined as the difference energy between the hard and easy axes of magnetization.

For hcp-Co, the average converged value is 250 K J m^{-3} using the GGA-PBE functional while the experimental value is 400 K J m^{-3}. This large difference has been already well documented in the works by Daalderop [51], Halilov [52] and Burkert [53]. Cobalt, due to its small anisotropy value represents a very good example to test the numerical convergence with respect to k-points.

For YCo_5 the converged value is ~7071 K J m^{-3} (3.7 meV) and the experimentally reported value is 6500 K J m^{-3}. Our calculated number is in agreement with the works of Daalderop [54] and Nguyen [55] which reportMAE values between 3 and 4 meV. For $SmCo_5$ we obtain a MAE of ~21 800 K J m^{-3} (~12 meV). Experimentally the reported value oscillate between 13 and 16 meV [56–59]. Other groups report values between 12.6 and 21.6 meV, including the study of Daalderop [54]. In sharp contrast to our results, the previous work by Larson–Mazin [60] not only wrongly determined the easy axis but overestimating MAE. This is due to the relatively poor k-sampling of only 180 k-points. In fact, as one can see from figure A1, more than 1000 k-points are needed to achieve convergence.

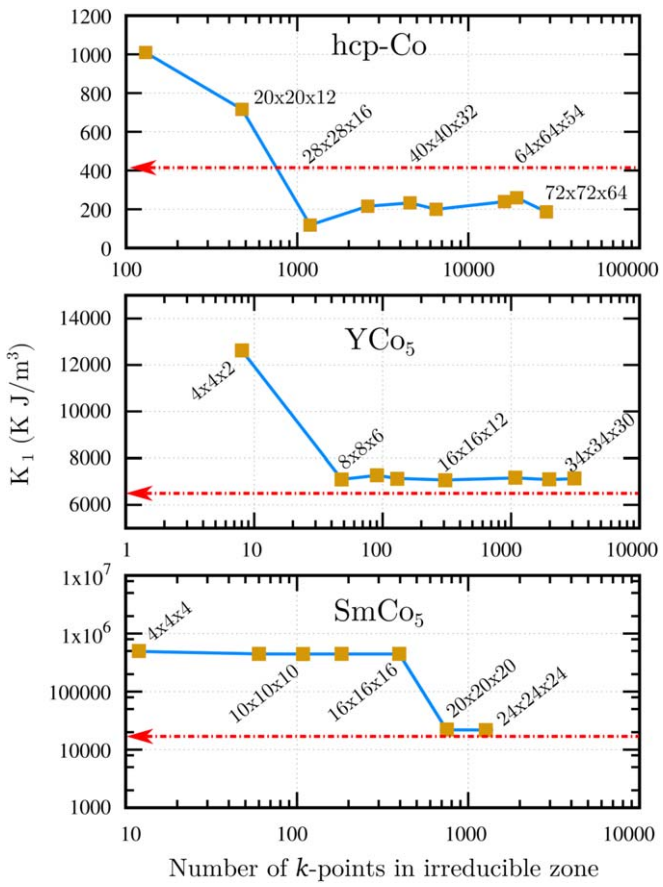

Figure A1. First-moment uniaxial (K_1) magnetic anisotropy energy (MAE) defined as the difference energy between the hard and easy axes of magnetization as q function of k-points. Dashed red lines are the experimental values taken from Coey [39].

ORCID iDs

José A Flores-Livas https://orcid.org/0000-0002-4183-1316
Silvana Botti https://orcid.org/0000-0002-4920-2370

References

[1] Nishihata Y, Mizuki J, Akao T, Tanaka H, Uenishi M, Kimura M, Okamoto T and Hamada N 2002 *Nature* **418** 164
[2] Deschler F *et al* 2014 *J. Phys. Chem. Lett.* **5** 1421
[3] Okuda T, Nakanishi K, Miyasaka S and Tokura Y 2001 *Phys. Rev.* B **63** 113104
[4] Liu M, Johnston M B and Snaith H J 2013 *Nature* **501** 395
[5] Lee M M, Teuscher J, Miyasaka T, Murakami T N and Snaith H J 2012 *Science* **338** 643
[6] Eerenstein W, Mathur N D and Scott J F 2006 *Nature* **442** 759
[7] Hur N, Park S, Sharma P A, Ahn J S, Guha S and Cheong S-W 2004 *Nature* **429** 392
[8] Ramirez A P 1997 *J. Phys: Condens. Matter* **9** 8171
[9] Beno M A, Soderholm L, Capone D W II, Hinks D G and Jorgensen J D 1987 *Appl. Phys. Lett.* **51** 57
[10] Wu M K, Ashburn J R, Torng C J, Hor P H, Meng R L, Gao L, Huang Z J, Wang Y Q and Chu C W 1987 *Phys. Rev. Lett.* **58** 908
[11] Zhang N, Yokota H, Glazer A, Ren Z, Keen D, Keeble D, Thomas P and Ye Z-G 2014 *Nat. Commun.* **5** 5231
[12] Flores-Livas J A, Tomerini D, Amsler M, Boziki A, Rothlisberger U and Goedecker S 2018 *Phys. Rev. Mater.* **2** 085201
[13] Xing G, Mathews N, Lim S S, Yantara N, Liu X, Sabba D, Grätzel M, Mhaisalkar S and Sum T C 2014 *Nature Mater.* **13** 476
[14] Kundu A K 2016 *Magnetic Perovskites: Synthesis, Structure and Physical Properties* (Berlin: Springer)
[15] Mitchell R H 2002 *Perovskites: Modern and Ancient* (Thunder Bay: Almaz Press)
[16] Ye Z-G 2008 *Handbook of Advanced Dielectric, Piezoelectric and Ferroelectric Materials: Synthesis, Properties and Applications* (Amsterdam: Elsevier)
[17] Fuertes A 2012 *J. Mater. Chem.* **22** 3293
[18] Bacher P, Antoine P, Marchand R, L'Haridon P, Laurent Y and Roult G 1988 *J. Solid State Chem.* **77** 67
[19] Zakutayev A 2016 *J. Mater. Chem.* A **4** 6742
[20] Brese N E and DiSalvo F 1995 *J. Solid State Chem.* **120** 378
[21] Sarmiento-Pérez R, Cerqueira T F T, Körbel S, Botti S and Marques M A L 2015 *Chem. Mater.* **27** 5957
[22] Amsler M and Goedecker S 2010 *J. Chem. Phys.* **133** 224104
[23] Goedecker S 2004 *J. Chem. Phys.* **120** 9911
[24] Medarde M L 1997 *J. Phys.: Condens. Matter* **9** 1679
[25] Marezio M, Remeika J P and Dernier P D 1970 *Acta Crystallogr. Sect.* B **26** 2008
[26] Antonov V N, Bekenov L V and Ernst A 2016 *Phys. Rev.* B **94** 035122
[27] Liferovich R P and Mitchell R H 2004 *J. Solid State Chem.* **177** 2188
[28] Afonso J F and Kuneš J 2017 *Phys. Rev.* B **95** 115131
[29] Chikazumi S and Graham C D 2009 *Physics of Ferromagnetism 2e* (Oxford : Oxford University Press) p 94
[30] Gschneidner K A 2016 *Handbook on the Physics and Chemistry of Rare Earths* vol 50, p 1 including Actinides
[31] Liechtenstein A I, Anisimov V I and Zaanen J 1995 *Phys. Rev.* B **52** R5467
[32] Czyżyk M T and Sawatzky G A 1994 *Phys. Rev.* B **49** 14211
[33] Bultmark F, Cricchio F, Grånäs O and Nordström L 2009 *Phys. Rev.* B **80** 035121
[34] Perdew J P and Wang Y 1992 *Phys. Rev.* B **45** 13244
[35] Jiang H, Gomez-Abal R I, Rinke P and Scheffler M 2009 *Phys. Rev. Lett.* **102** 126403
[36] Essenberger F, Sharma S, Dewhurst J K, Bersier C, Cricchio F, Nordström L and Gross E K U 2011 *Phys. Rev.* B **84** 174425
[37] Peil O E, Ferrero M and Georges A 2014 *Phys. Rev.* B **90** 045128
[38] Matsushita Y-I, Madjarova G, Flores-Livas J A, Dewhurst J K, Felser C, Sharma S and Gross E K 2017 *Ann. Phys., Lpz.* **529** 1600412
[39] Coey J M 2010 *Magnetism and Magnetic Materials* (Cambridge: Cambridge University Press)
[40] Björkman T 2011 *Comput. Phys. Commun.* **182** 1183
[41] Stevanović V, Lany S, Zhang X and Zunger A 2012 *Phys. Rev.* B **85** 115104
[42] Sarmiento-Pérez R, Botti S and Marques M A 2015 *J. Chem. Theory Comput.* **11** 3844
[43] Togo A and Tanaka I 2015 *Scr. Mater.* **108** 1
[44] Miao G-X and Moodera J S 2015 *Phys. Chem. Chem. Phys.* **17** 751
[45] Zhao H J, Bellaiche L, Chen X M and Íñiguez J 2017 *Nat. Commun.* **8** 14025
[46] Perdew J P, Burke K and Ernzerhof M 1996 *Phys. Rev. Lett.* **77** 3865
[47] Kresse G and Furthmüller J 1996 *Comput. Mater. Sci.* **6** 15
[48] Ong S P, Richards W D, Jain A, Hautier G, Kocher M, Cholia S, Gunter D, Chevrier V L, Persson K A and Ceder G 2013 *Comput. Mat. Sci.* **68** 314
[49] Dewhurst K *et al* 2015 The Elk FP-LAPW Code http://elk.sourceforge.net/
[50] Lejaeghere K *et al* 2016 *Science* **351** aad3000
[51] Daalderop G H O, Kelly P J and Schuurmans M F H 1990 *Phys. Rev.* B **41** 11919
[52] Halilov S V, Perlov A Y, Oppeneer P M, Yaresko A N and Antonov V N 1998 *Phys. Rev.* B **57** 9557
[53] Burkert T, Eriksson O, James P, Simak S I, Johansson B and Nordström L 2004 *Phys. Rev.* B **69** 104426
[54] Daalderop G, Kelly P and Schuurmans M 1996 *Phys. Rev.* B **53** 14415
[55] Nguyen M C, Yao Y, Wang C-Z, Ho K-M and Antropov V P 2017 arXiv:1706.07368
[56] Szpunar B 1981 *Acta Physica Polonica.* A **60** 791
[57] Zhao T-S, Jin H-M, Grössinger R, Kou X-C and Kirchmayr H 1991 *J. Appl. Phys.* **70** 6134
[58] Leslie-Pelecky D L and Schalek R L 1999 *Phys. Rev.* B **59** 457
[59] Chen C H, Walmer M S, Walmer M H, Gong W and Ma B-M 1999 *J. Appl. Phys.* **85** 5669
[60] Larson P, Mazin I and Papaconstantopoulos D 2003 *Phys. Rev.* B **67** 214405